energies

MDPI

Article

Kinetic Model Implementation of Fluidized Bed Devolatilization

Armando Vitale, Andrea Di Carlo *, Pier Ugo Foscolo and Alessandro Antonio Papa

Industrial Engineering Department, University of L'Aquila, Piazzale E. Pontieri 1, Monteluco di Roio, 67100 L'Aquila, Italy; armando.vitale@graduate.univaq.it (A.V.); pierugo.foscolo@univaq.it (P.U.F.); alessandroantonio.papa@univaq.it (A.A.P.)

* Correspondence: andrea.dicarlo1@univaq.it

Abstract: Computational modeling is a powerful tool for studying and investigating the behavior of fluidized bed gasifiers and the modeling of the initial devolatilization step is necessary to provide a reliable description of the whole process involving the feedstock decomposition and the subsequent gasification reaction. In this work, a bench-scale fluidized bed reactor was used to examine the devolatilization of different carbonaceous materials within the temperature range from 650 to 850 °C. The experimental test campaign was used to derive the linear correlation factor to describe the devolatilization in terms of product distribution as a function of temperature and highlight the different behavior between lignocellulosic and plastic feedstocks. Furthermore, the experimental data were used to develop concise kinetic expressions able to fit the experimental devolatilization times ranging from 75 in the case of poplar at a lower temperature and 22 s for the Organic Fraction of Municipal Solid Waste (OFMSW) at a higher temperature. The obtained model produces a simple kinetic expression where the size of the particle is enclosed in the kinetic parameters. The kinetic model sided by the application of linear correlations describes the overall thermal decomposition in a fluidized bed, simplifying its modeling in commercial simulation software, even when particles are considered as point-like bodies.

Keywords: devolatilization; gasification; polypropylene; biomass; lignocellulosic material; kinetic model

Citation: Vitale, A.; Di Carlo, A.; Foscolo, P.U.; Papa, A.A. Kinetic Model Implementation of Fluidized Bed Devolatilization. *Energies* **2024**, *17*, 3154. https://doi.org/10.3390/en17133154

Academic Editors: Shaofei Zheng, Jian Liu, Liu Liu, Han Shen, Bengt Sunden and Xiaodong Wang

Received: 29 May 2024
Revised: 22 June 2024
Accepted: 24 June 2024
Published: 26 June 2024

1. Introduction

The world's population is predicted to expand by about 2 billion people during the next 30 years, from the present 8 billion to 9.7 billion in 2050, and might peak at approximately 10.4 billion in the mid-2080s [1]. The population growth is closely linked to the increasing energy demand, which comes mainly from industrial development, a key driver of economic growth. Currently, the energy need is mainly met through fossil fuel sources [2]. Industrial development increases power consumption and also raises the need for reliable and affordable energy sources; however, this increase in energy consumption may result in greater greenhouse gas emissions unless mitigated by cleaner technologies and efficiency improvements in industrial processes.

Since the extraction and conversion of fossil fuels depletes the planet's natural resources and produces harmful greenhouse gases, resulting in environmental concerns, one solution is the conversion of various renewable or recyclable raw materials, such as waste, biomass, or even mixtures of them to produce energy in a sustainable way. Thermochemical conversions could be an essential part of a sustainable and integrated biomass and waste management system, as they are suitable routes to produce energy and fuels from feedstocks and waste materials [3–5].

Gasification is one of the most well-known waste-to-energy (WtE) processes among traditional thermochemical approaches [6,7]. By subjecting residues to high temperatures that break down molecules into their constituent parts in an oxygen-deficient environment, gasification creates a final gas made up of H_2, CO, CO_2, CH_4, and short-branched

hydrocarbons that can then be used to generate power, chemicals, hydrogen, and liquid fuels [4,8–12].

The fundamental steps in complex thermochemical conversions include the devolatilization process: it consists of the high-temperature primary decomposition of the material, which takes place before the volatiles emitted are subjected to homogeneous and heterogeneous reactions in the ambient space surrounding the particles. The devolatilization kinetic is mainly a function of the nature of the solid fuel, particle size, and associated temperature gradients; it deeply influences the final products of the gasification process. However, numerical routines available to simulate the behavior of gasifiers consider particles as point-like entities (with zero dimensions), so they fail a reliable, generalized description of devolatilization under changing operating conditions [13,14].

Fluidization is the most promising technology in biomass and waste gasification: it has high mixing capabilities, in addition to a high mass and heat transfer rate, which ensures uniform temperatures throughout the gasifier; additionally, catalysts can be used as part of the gasifier bed, directly impacting tar reforming [10,11].

Due to the high temperatures and rough movements of the bed material, investigating fluid mechanics inside a fluidized bed system is a difficult task. Hydrodynamic experiments have only been conducted using cold flow modeling which excludes heat transfer processes and chemical reactions. Devolatilization methods, in particular for biomass and waste gasification, alter bed hydrodynamics, because volatiles are released inside the bed and influence particle mobility [15].

Fluid dynamics computational models are a powerful tool for investigating the hydrodynamics inside fluidized bed reactors, and the accuracy of predictions has improved significantly in recent decades.

To correctly describe the gasification process, the introduction of the initial devolatilization phase results to be crucial, it represents an essential step that influences the system from both a fluid dynamics and chemical point of view due to the solid decomposition and compounds released.

In fact, in the description of the gasification, the solid decomposition, the residence times, and the distribution of the released compounds, that subsequently are involved in chemical reactions within the oxidative environment, are considered as key elements.

Several research efforts on the devolatilization process have been published in the literature [16,17]; these studies appear to be primarily concerned with the examination of product distribution in volatile gas, tar, and char. Such qualitative and quantitative assessments are supplemented by studies on the thermal degradation process, which is frequently described by exceedingly complex kinetics [18].

Further kinetic investigations are instead carried out using mass loss in TGA or experiments performed in different types of reactors; the kinetics derived in these circumstances do not, therefore, reflect the true behavior of the particle within a fluidized bed [15,19–21].

In this study, five materials were tested in a bench-scale fluidized bed reactor to achieve a more realistic simulation of devolatilization kinetics in a fluidized bed enclosing the thermal exchange phenomena.

The form of these kinetic expressions (modified Arrhenius law) agrees with those found in the literature and with those implementable in several CFD software programs like Barracuda CPFD software or Ansys [15,19,21], that are examples of CFD modeling software.

This work was motivated by the desire to close a gap in the literature about the simulation of the devolatilization of various materials using fluidized bed reactors. The experimental data were utilized to define product distributions and to create a kinetic model of the thermal decomposition process (called DEV_Model), which may be incorporated in modeling software to improve the simulation predictions regarding gasification.

By utilizing the expressions described in this study, it is possible to simulate the devolatilization process in fluidized beds within modeling software, while also predicting the behavior and distribution of products at temperatures between those evaluated experimentally.

2. Materials and Methods

2.1. Materials

Several feedstocks were used in the experimental tests in this work, including 3D printed polypropylene (PP) spheres and biomasses such as poplar, wheat straw, almond shells, and OFMSW (Organic Fraction Municipal Solid Waste) that were milled, dried, and pelletized.

The PP spheres with 10 mm diameters were printed with Ultimaker PP ® filament using an UltiMaker s3® printer (Ultimaker B.V., Geldermanse, The Netherlands). The biomasses were instead pelletized to have a comparable size with PP spheres.

Figure 1 shows an example of a 3D printed PP sphere and tablets for biomass.

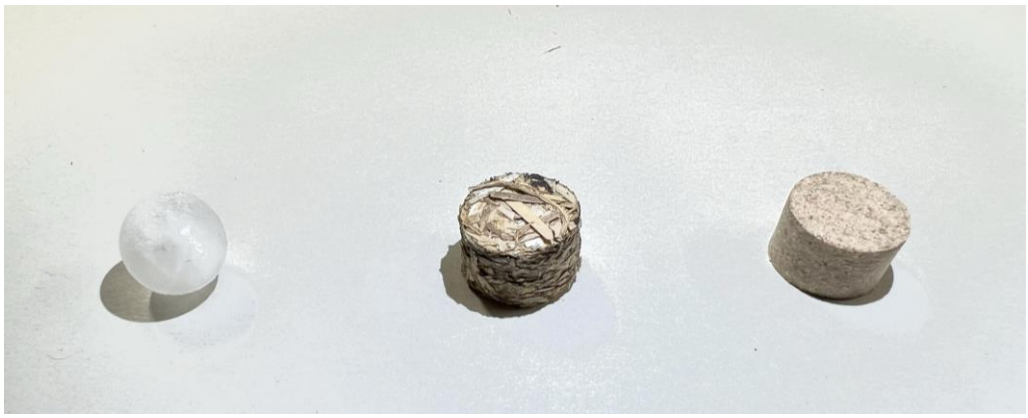

Figure 1. Example of feedstock samples (polypropylene, wheat straw, and poplar from left to right).

The materials were chosen to provide a broad overview of the variability of feedstock for gasification.

Polypropylene is an example of plastic waste, OFMSW is representative of organic waste, and the other samples are examples of various types of biomass.

Table 1 shows the average particle mass utilized for tests, ash content, and data acquired from ultimate analysis of dried samples.

Table 1. Ultimate analysis of tested materials.

	Weight (g)	C (%) *	H (%) *	N (%) *	S (%) *	O (%) *	Ash (%) **
Polypropylene	0.473	49.0%	6.0%	0.2%	0.0%	43.0%	0.70%
Poplar	0.519	49.3%	6.0%	0.2%	0.0%	43.3%	1.24%
Wheat straw	0.423	36.0%	5.1%	0.0%	0.6%	39.4%	18.94%
Almond shells	0.529	47.0%	6.4%	0.0%	0.7%	43.5%	2.40%
OFMSW	0.320	46.3%	7.4%	2.0%	0.9%	40.2%	3.25%

* dry, ash-free; ** dry.

2.2. Bench Scale Experimental Apparatus and Operational Procedure

The devolatilization tests were performed using the lab-scale facility reported in Figure 2 and accurately described in a previous work [22]. Specifically, the decomposition occurs inside a fluidized bed reactor with a bed material of quartz sand particles having a density of 2.65 g/cm^3 and a Sauter's diameter of 222 µm.

Table 2 reports the minimum fluidization velocity based on the sand characteristics, as well as the nitrogen flow rate required to maintain a velocity equal to twice the minimum fluidization velocity ($2 \times u_{mf}$) at the different temperatures selected for the tests.

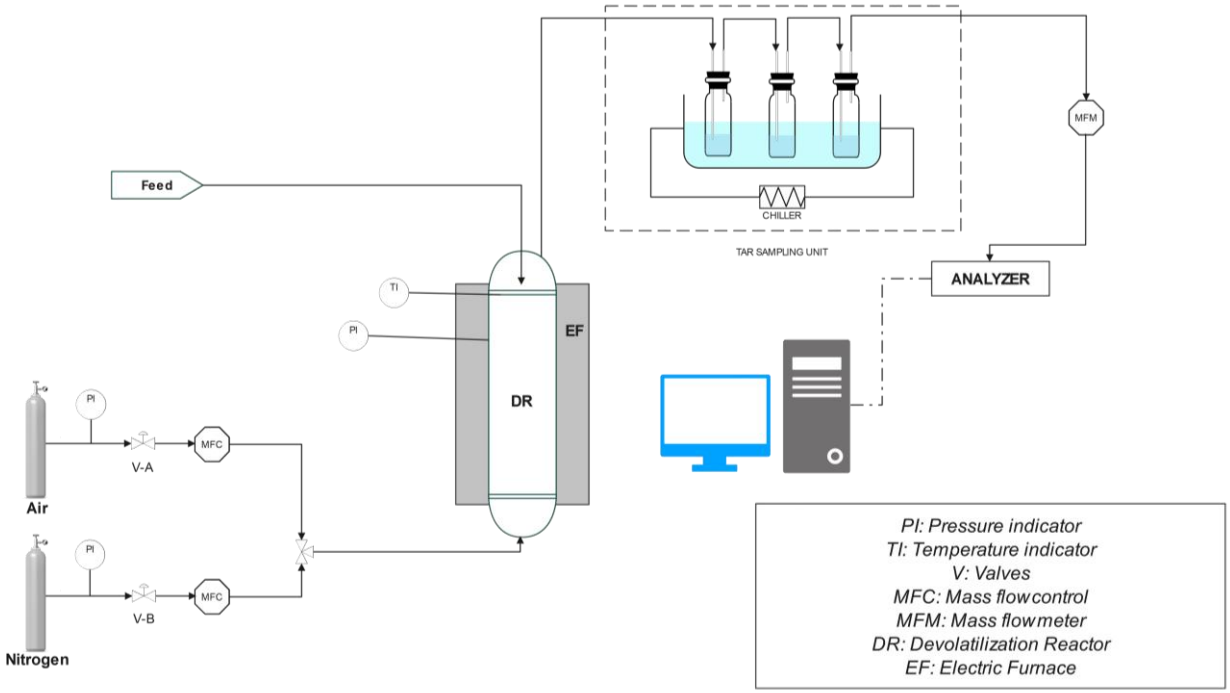

Figure 2. Schematic diagram of devolatilization test plant.

Table 2. Minimum fluidization velocity and reactor operating flow rates.

Temperature (°C)	Minimum Fluidization Velocity (m/s)	Experimental N_2 Flow Rate (~2u_{mf}-Nl/min)
650	2.52×10^{-2}	2.07
750	2.37×10^{-2}	1.76
850	2.24×10^{-2}	1.51

The experimental apparatus consists of a fluidized bed reactor heated up by an electrical furnace that allows for the maintenance of a stable working temperature during the tests. The chosen flow rate of nitrogen and air were fed by means of a mass flow controller (Bronkhorst) during devolatilization and combustion phases, respectively. The gaseous products were analyzed in terms of flow rate (measured by a Bronkhorst mass flow meter) and composition (H_2, CO, CO_2, and CH_4) measured by ABB analyzers (Caldos and Uras).

The condensable compounds were trapped with the use of isopropanol traps and subsequently identified and quantified by the use of GC/MS (Gas Chromatography with Mass Spectrometry, Agilent 7890, Agilent Technologies, Inc., Santa Clara, CA, USA).

The presence of the small fraction of evolved volatiles in the reactor ensures the in-depth study of the decomposition of the fuel material by limiting the presence of reactions outside the particle.

The experiments were carried out with the same procedure reported in the previous work but in this case using a wider selection of feedstock [22].

Tests start with the injection from the top of the reactor and the subsequent decomposition of the feedstock to analyze the gas released during the devolatilization phase.

After the devolatilization phase, air instead nitrogen was fluxed inside the reactor with the same fluidization condition to perform the combustion and estimate the char term that represents the residual after the devolatilization.

By performing the complete series of tests and replications for each material and reactor temperature, it is possible to identify the products' distribution and derive the kinetic expressions that describe the devolatilization process for each material, furnishing a parametric study based on the main variable that is the working temperature.

2.3. Mathematical Model of the Devolatilization Process (DEV_Model)

The approach adopted for the model is substantially simpler than the one previously developed and in general simpler than the reaction mechanism applied for solid decomposition, being based on the first-order kinetic mechanism commonly used for homogeneous reactions [22].

The conversion process is characterized by an apparent activation energy and a pre-exponential factor where the external and intra-particle mass transfer resistances are incorporated into the overall kinetic expression [23]. The endothermic and exothermic reaction routes are considered to be in a state of thermal equilibrium so that the entire variation in the enthalpy of devolatilization may be neglected. This assumption of a thermo-neutral process is extensively used in the scientific literature, even in more advanced models [24].

Of particular interest is the pre-exponential factor used in the kinetic equation; it is expressed through a power law function of the temperature, with this factor being necessary for fitting the experimental data.

The feedstocks are modeled as the equivalent spheres having the same mass as the pellet, calculating the equivalent diameter according to the following equation:

$$R_P = \sqrt[3]{\frac{3}{4}\frac{V_{pellet}}{\pi}} \tag{1}$$

As in the previous work, the starting point for modeling comes from the equations of the conservation of mass and energy and it is based on the same assumption [22,25].

$$\rho_p C_p \frac{\partial T}{\partial t} = \frac{1}{r^2}\frac{\partial}{\partial r}\left(r^2 k_{eff}\frac{\partial T}{\partial r}\right) \tag{2}$$

This equation is solved with the initial condition and boundary conditions shown below. The boundary conditions on the particle surface consider the heat exchange by convection and radiation up to the bed temperature.

$$\text{IC} \qquad \begin{matrix} T(t=0) = 20^{\circ}\text{C} \\ 0 \le r \le R_p \end{matrix} \tag{3}$$

$$\text{BCs} \qquad k_{eff}\left.\frac{\partial T}{\partial r}\right|_{r=R_p(t)} = h(T_b - T) + \sigma\epsilon_{eff}\left(T_b^4 - T^4\right) \tag{4}$$

$$k_{eff}\left.\frac{\partial T}{\partial r}\right|_{r=0} = 0 \qquad t > 0 \tag{5}$$

The apparent devolatilization kinetics for a particle, in accordance with the concepts expressed above, can then be described by the following differential expression, in terms of conversion, which includes pseudo first-order kinetics [26]:

$$\frac{d\chi}{dt} = K_d(1 - \chi(t)) \tag{6}$$

The kinetic "constant", K_d, is calculated as a function of temperature according to the equation below:

$$K_d(T) = A_d exp\left(-\frac{E_d}{RT}\right) \tag{7}$$

As mentioned above, the pre-exponential factor A_d appearing in Equation (7) depends on the temperature:

$$A_d = C_1(T)^{C_2} \tag{8}$$

Linked to the conversion equation, there is the differential equation that expresses the mass consumption, expressed below:

$$\frac{dm}{dt} = -K_d m(t) \tag{9}$$

Matlab® software (Update 6 Version 23.2.0.2485118 (R2023b); The MathWorks Inc., Natick, MA, USA) was used to solve the equations; in particular, the symbolic math toolbox was used to solve the differential equation for mass consumption and conversion, the PDEPE function was used to solve the heat transfer equation, and the optimization toolbox was used to estimate the kinetic parameters.

A spatial and time domain discretization was built to solve Fourier's law with the PDEPE function, and this discretization was utilized to determine the variation in the temperature profile inside the particle as a function of time. To derive the mean particle temperature as a function of time, the obtained values were mediated along the particle radius.

This type of calculation was used to insert the dimension of the feed as an important parameter in the devolatilization process and to allow it to influence the devolatilization process.

The consideration of fuel particle size dependence within the kinetic parameters, as shown above, thus also allows taking into account this parameter within the CFD software. As a matter of fact, in most numerical models for fluidized bed reactors, the particles are treated as point-like bodies and thus the size fluctuation cannot be taken into consideration, whereas in this approach, the initial calculation of Fourier's law allows for the influence of fuel particle size in the heating phase, which then affects the estimation of the kinetic parameters; the following averaging operation is rather used to allow for the introduction of the temperature parameter into the kinetic equations.

Such heat transfer considerations are reported in the literature and are allowed for, when convective heat transfer in the shrinking core model is highly relative to conductive heat transfer and a high pyrolysis rate occurs simultaneously [27].

The temperature profile within the particle as a function of time was calculated as the starting point for solving the DEV_Model, followed by the calculation of the average temperature of the whole particle.

Using the Matlab FIT function, an exponential formula consisting of two terms was developed to express the trend of the particle average temperature as a function of time.

This expression was then incorporated into the mathematical expressions obtained from the symbolic resolution of the conversion and mass consumption equations.

The A_d and E_d parameters were then determined for each temperature and material combination using the Matlab Optimization Toolbox.

The A_d and E_d parameters were found by setting the solid conversion in the equations to 99% at the experimentally determined devolatilization time t_d.

This procedure was conducted for each material and temperature, and then the A_d and E_d parameters were averaged for each individual material. Equation (8) was used to determine the relation of A_d as a function of temperature. In particular, the C_1 and C_2 parameters were derived by utilizing the FIT function of Matlab once more.

Summarizing the reported model produces an easier kinetic expression where the size of the particle is enclosed in the kinetic parameters and represents an improvement in the previously developed model [22].

The obtained expression is more convenient to use and easier to implemented in commercial software or in more complex numerical models.

3. Results and Discussion

Figures 3 and 4 show the typical trends of reactor outlet gas composition, measured by ABB analyzers, obtained during the devolatilization phase (Figure 3) and the combustion phase (Figure 4): the experiments with polypropylene are depicted. Similar graphs, with the presence of CO and CO_2 this time, were obtained for the other materials.

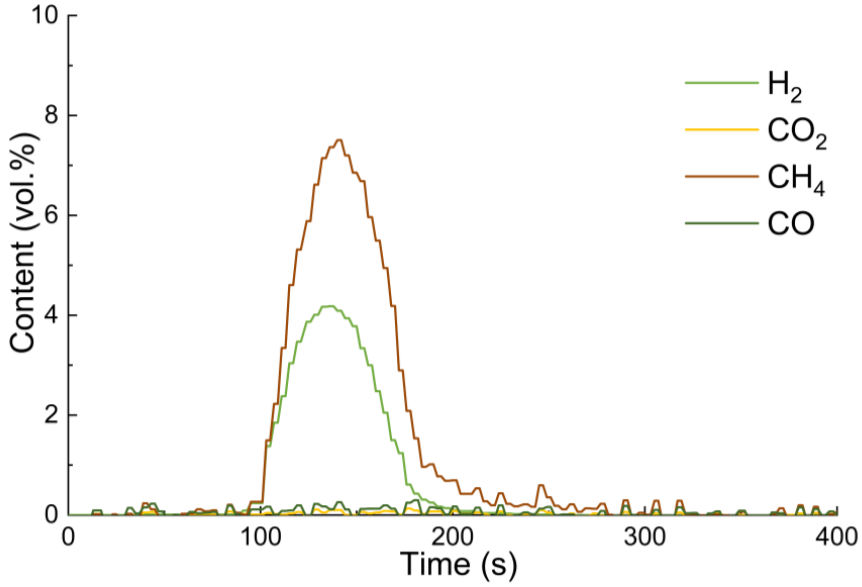

Figure 3. Trend of volume percentages of gases during the devolatilization step of polypropylene spheres, measured by ABB analyzer.

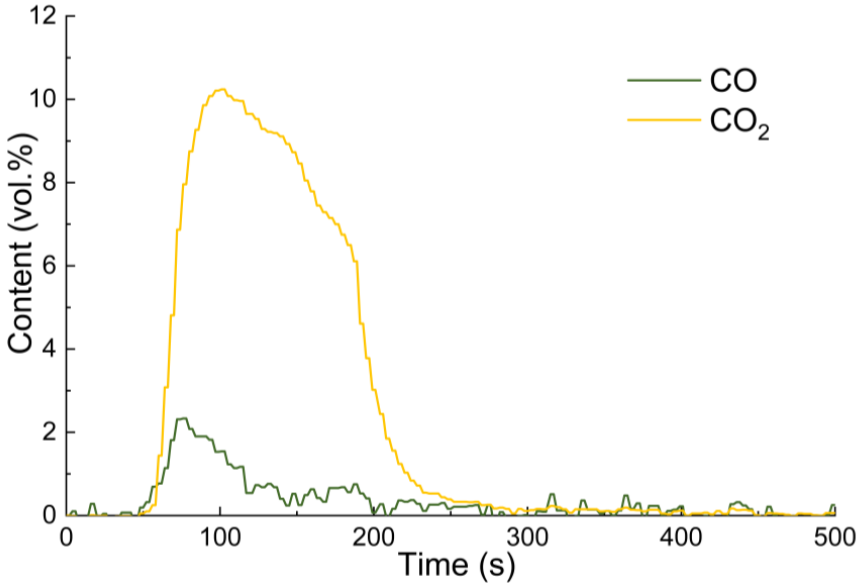

Figure 4. Trend of volume percentages of gases during the combustion step, measured by ABB analyzer.

Knowing the composition and flow rate of produced gas, measured by MFM, it was possible to derive the molar flow rates of gaseous species obtained. By integration of the curves, the whole amount of gas produced in each test was derived. The initial time values shown on the abscissa in Figures 3 and 4 are arbitrary values.

Each test generates a response that is the product of the devolatilization process dynamics as well as the impacts of mixing and transport delays. Connecting wires with a high length-to-inner diameter ratio were employed to prevent axial mixing. The elimination of external effects was carried out by performing tests on residence times with tracer gas (CO_2) according to the procedure reported in the literature [22,28].

The following outcomes were achieved using the previously mentioned technique. An important aspect of the research is the distribution of products from the devolatilization process.

Figure 5 shows the weight percentages of the individual products obtained for each material tested and at the temperatures reported above (Table 2).

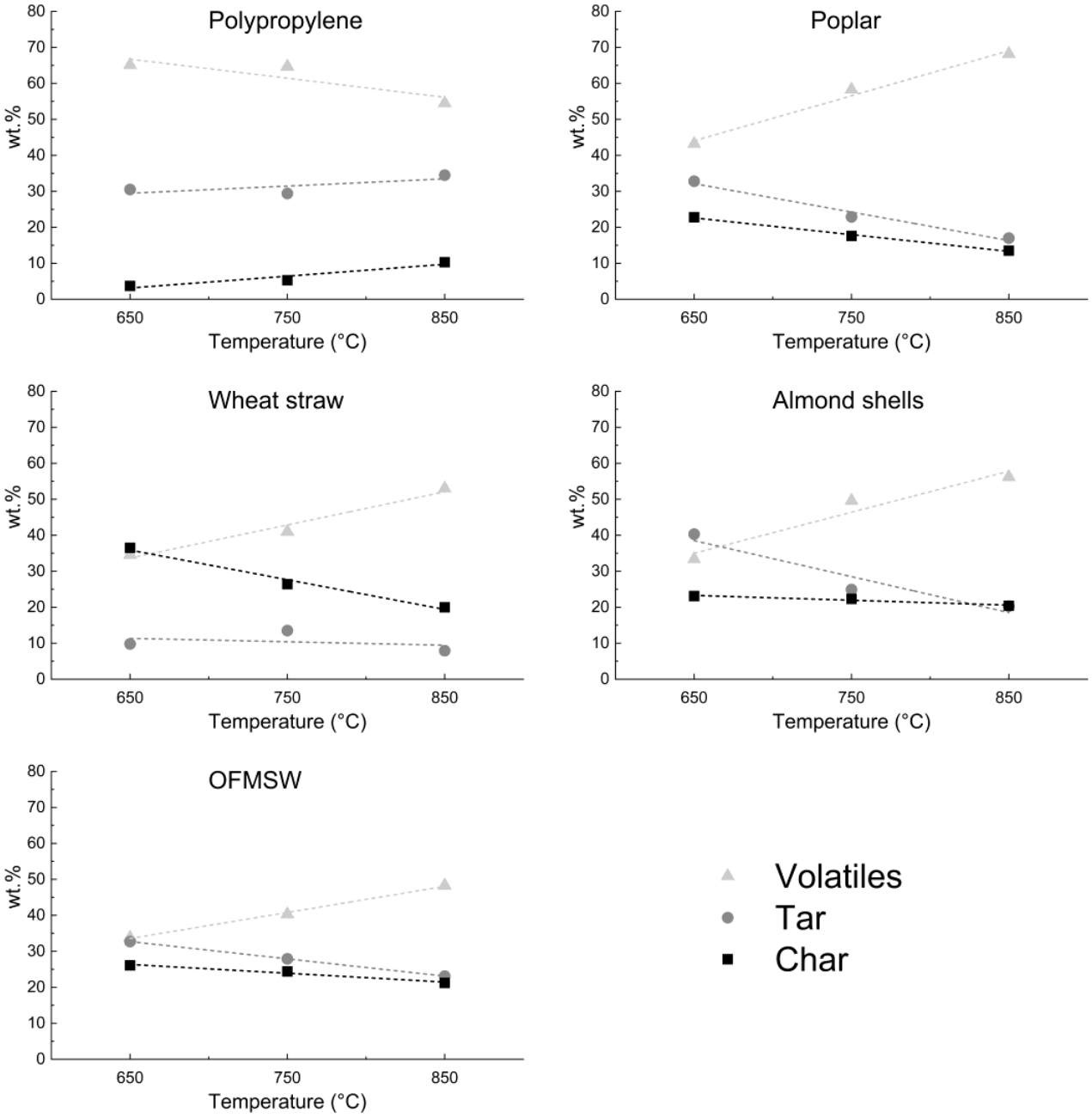

Figure 5. Trend of weight percentages of devolatilization products.

The subdivision of products is made into volatile, tar, ash, and char measured as described above. The ash term encloses the portion of sulfur and nitrogen content in the sample, while the tar term includes the heavy hydrocarbons measured in the tar sampling unit and the portions of unmeasured compounds, obtained by mass balances. Figure 5 excludes previously reported percentages of ash.

It is easy to observe the different trends with temperature of lignocellulosic feedstocks with respect to plastic material as shown in Figure 5.

In particular, OFMSW, poplar wheat straw, and almond shell present an increase in the volatile fraction with the increase in the working temperature and a parallel drop in the tar and char terms.

For polypropylene, the trend is the opposite, as visible in Figure 5 and highlighted by the coefficient reported in Table 3.

Table 3. Fitting parameters for products' distribution.

Volatiles	**a**	**b**
Polypropylene	−0.053	115.65
Poplar	0.125	−71.308
Wheat straw	0.092	−51.249
Almond shells	0.0114	−70.222
OFMSW	0.0725	−33.368
Tar	**c**	**d**
Polypropylene	0.02	11.007
Poplar	−0.0465	65.536
Wheat straw	−0.0095	20.119
Almond shells	−0.0135	35.774
OFMSW	−0.0245	48.964
Char	**e**	**f**
Polypropylene	0.033	−27.326
Poplar	−0.079	105.05
Wheat straw	−0.0825	112.03
Almond shells	−0.1	130.8
OFMSW	−0.048	77.004

As widely described in the literature, the high-temperature decomposition of lignocellulosic materials leads to a deep breaking of the reticular structure of cellulose, hemicellulose, and lignin resulting in a lower char yield and higher light compound production [29,30].

For polypropylene, the opposite trend in the char and tar terms may be attributed to the presence of undesired recombination reactions (Diels–Alder reactions [31]) between the more unstable molecules produced by the radical chain scission that represents the main mechanism for polyolefins' thermal degradation [32].

Regarding the polypropylene volatile fraction, the yield reduction can also be related to the improved quality of the gas. In fact, as shown in the following, the hydrogen production increased with temperature, while the methane decreased, leading to a reduction in terms of gas yield.

Furthermore, the data obtained, as shown in Figure 5, allow us to easily describe the products' distribution by equations with a linear correlation factor as follows:

$$Volatiles(\text{wt\%}) = aT + b \tag{10}$$

$$Tar(\text{wt\%}) = cT + d \tag{11}$$

$$Char(\text{wt\%}) = eT + f \tag{12}$$

where T is the temperature expressed in Kelvin. The parameters of the fitting equations are reported in Table 3.

Taking advantage of the equations and parameters just expressed, it is then possible to derive the product distribution for intermediate temperatures as well.

The volatile compounds are then characterized in terms of gas species measured by ABB analyzers, as illustrated in Figure 6.

Again, specific trends can be observed for volatile compounds; as temperature increases, there is an increase in the percentage of hydrogen for all the materials tested.

Analyzing the CO term, it remains stable for all lignocellulosic materials with the temperature change as well as the CH_4 one; regarding the CO_2, it slightly decreases with the opposite trend with respect to H_2.

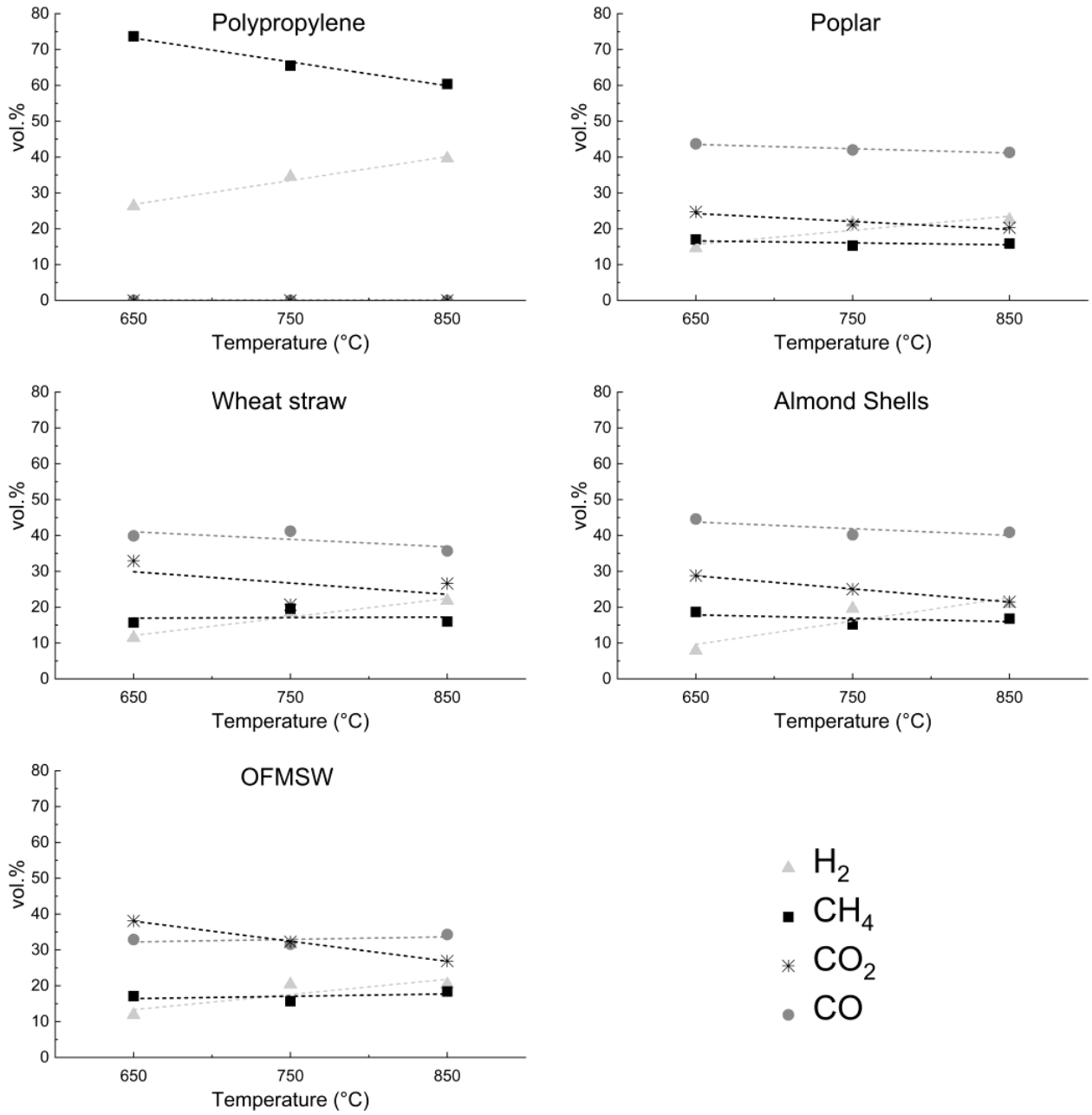

Figure 6. Trend vs. temperature of weight percentages of volatiles for all feedstocks.

Similarly to the distribution of products, fitting is carried out with the equations described below, whose parameters are shown in Table 4.

$$H_2(\text{wt\%}) = gT + h \tag{13}$$

$$CO(\text{wt\%}) = lT + m \tag{14}$$

$$CH_4(\text{wt\%}) = nT + p \tag{15}$$

$$CO_2(\text{wt\%}) = qT + v \tag{16}$$

Thus, by coupling the equations for products with those for volatile compounds, one can accurately describe devolatilization.

The measured composition of the most abundant aromatic compounds is reported in Table 5.

Table 4. Fitting parameters for volatiles' distribution.

H_2	g	h
Polypropylene	0.0665	−34.563
Poplar	0.0395	−20.842
Wheat straw	0.0515	−35.418
Almond shells	−0.0365	62.44
OFMSW	0.0425	−25.911
CO	**l**	**m**
Polypropylene	0	0
Poplar	−0.012	54.609
Wheat straw	−0.021	60.416
Almond shells	−0.0185	60.826
OFMSW	0.007	25.772
CH_4	**n**	**p**
Polypropylene	−0.0665	134.56
Poplar	−0.0055	21.693
Wheat straw	0.0015	15.566
Almond shells	−0.0095	26.619
OFMSW	0.0065	10.417
CO_2	**q**	**v**
Polypropylene	0	0
Poplar	−0.022	44.539
Wheat straw	−0.0315	58.958
Almond shells	0.065	−50.362
OFMSW	−0.056	89.721

Table 5. Tar and benzene weight percentages.

	Phenol [wt.%]	Naphtalene [wt.%]	Styrene [wt.%]	Xylene [wt.%]	Toluene [wt.%]	Benzene [wt.%]
Polypropylene						
650 °C	0.00%	7.26%	4.30%	24.25%	40.62%	23.56%
750 °C	0.00%	7.75%	7.55%	6.14%	27.03%	51.53%
850 °C	0.07%	17.85%	10.84%	1.62%	14.15%	55.48%
Poplar						
650 °C	6.26%	6.27%	10.43%	9.18%	36.30%	31.57%
750 °C	3.22%	7.38%	9.88%	5.75%	27.07%	46.70%
850 °C	4.26%	20.56%	10.23%	3.30%	18.62%	43.03%
Wheat straw						
650 °C	0.00%	7.42%	11.94%	9.40%	42.56%	28.68%
750 °C	0.00%	9.58%	14.18%	7.57%	33.21%	35.46%
850 °C	0.00%	15.42%	10.32%	3.60%	20.52%	50.14%
Almond shells						
650 °C	11.48%	5.15%	10.02%	9.91%	35.73%	27.71%
750 °C	1.64%	7.15%	10.17%	4.87%	29.55%	46.62%
850 °C	2.12%	20.71%	12.34%	4.17%	25.24%	35.42%
OFMSW						
650 °C	0.00%	7.96%	12.38%	9.29%	42.28%	28.09%
750 °C	0.00%	7.61%	10.93%	5.10%	33.77%	42.60%
850 °C	0.00%	7.61%	10.93%	5.10%	33.77%	42.60%

As already mentioned, this term also includes unmeasured compounds, which are considered as aromatic hydrocarbons with the aim of having a conservative approach.

Using the data in the figures and tables above, the following equations are obtained to introduce products' distribution for each material into the software model:

$$Feed \xrightarrow{Devolatilization} \alpha_1 Volatiles + \alpha_2 Tar + \alpha_3 Char + \alpha_4 Ash \quad \sum \alpha_i = 1 \tag{17}$$

$$Volatiles \rightarrow \beta_1 H_2 + \beta_2 CO + \beta_3 CH_4 + \beta_4 CO_2 \quad \sum \beta_i = 1 \tag{18}$$

Similarly to volatile chemicals, the term tar can be subdivided into the various compounds generated, as follows:

$$Tar \rightarrow \sum \gamma_i compound = 1 \tag{19}$$

These results offer a comprehensive overview of the products released during the devolatilization process; this knowledge is fundamental to carry out subsequent investigations of the whole gasification process and to simulate it numerically.

Data on the time intervals required for complete devolatilization of the samples were also obtained from the experimental tests and shown in Figure 7.

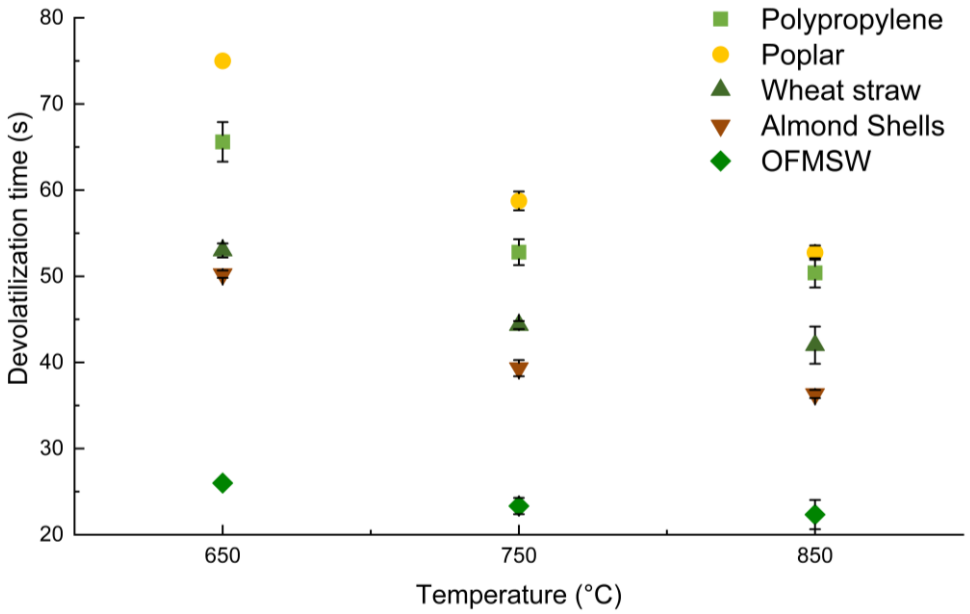

Figure 7. Experimental devolatilization times.

As mentioned above, these time interval values were derived by analyzing the curve describing the release of gases during the devolatilization process.

Figure 7 allows us to compare the devolatilization times of the various materials tested; poplar devolatilization is the slowest, followed by polypropylene, grain, almond shells, and finally OFMSW, which devolatilizes extremely fast.

This factor is influenced by the nature of the bonds inside the solid particles and the quality of the biomass and will naturally influence the kinetic parameters as discussed below.

Utilizing the equations and the procedure described above, in the section about the DEV_Model, and knowing the values reported in Figure 7, the kinetic parameters required for modeling the devolatilization phenomenon were derived (Table 6).

The activation energies appear to assume very close values, while the C1 parameter, which affects the pre-exponential factor, appears to be highly variable and is especially high in the case of rapid devolatilization.

Table 6. Kinetic parameters derived by using the DEV_Model.

	C1	*C2*	E_d
Polypropylene	7.126×10^5	−1.836	2.748×10^4
Poplar	3.665×10^4	−1.423	2.745×10^4
Wheat straw	4.070×10^6	−2.061	2.744×10^4
Almond shells	1.238×10^5	−1.543	2.741×10^4
OFMSW	4.308×10^7	−2.303	2.754×10^4

An example of the thermal profile inside the particle and as a function of time is shown in Figure 8 in order to obtain a comprehensive view of the mathematical modeling; in particular, it has been referred to as the polypropylene sphere.

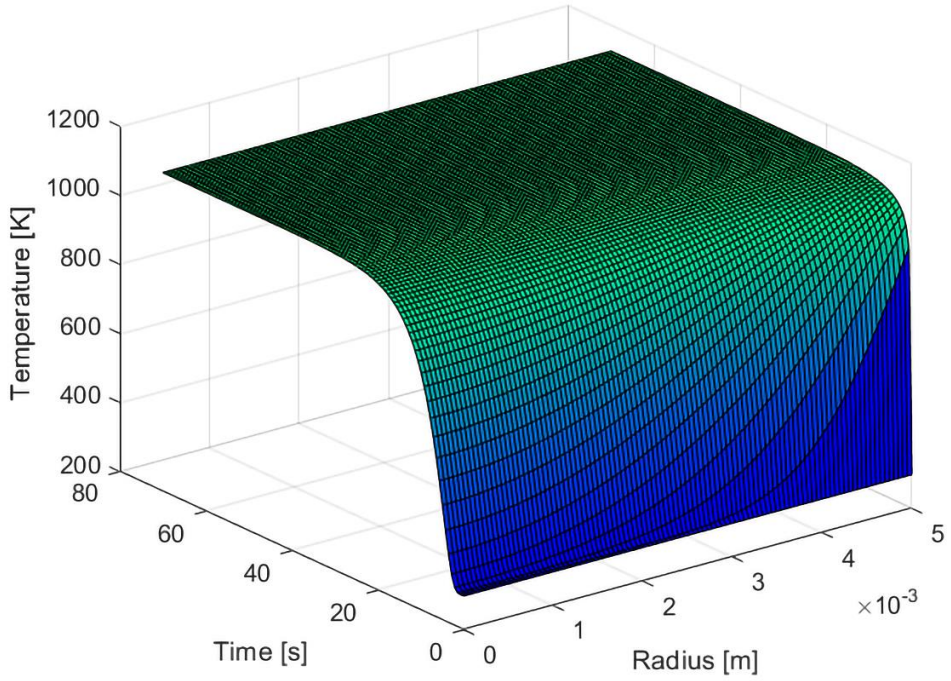

Figure 8. Temperature profile within the PP particle as time changes.

This figure shows the spatial and temporal discretization used by the PDEPE function.

Figure 8 is also complemented by Figure 9 which shows the calculated particle average temperature as a function of time.

Figure 9 is obtained, as already shown, averaging along the radius the values of Figure 8.

Finally, for completeness, graphs showing the conversion trend for each material as a function of time, parameterized by temperature, are shown.

Figure 10 shows the devolatilization trend described by the kinetic model for each material and temperature, where the accuracy of the model in the devolatilization times' prevision can also be seen.

As shown in Figure 7, the temperature affects the degradation times less for some materials than for others (e.g., OFMSW). This behavior is reflected in the trends predicted by the model, where the temperature-dependent conversion curves almost overlap. This behavior is probably due to the fast heating of the particle, where the limiting stage appears to be chemical decomposition and not heating.

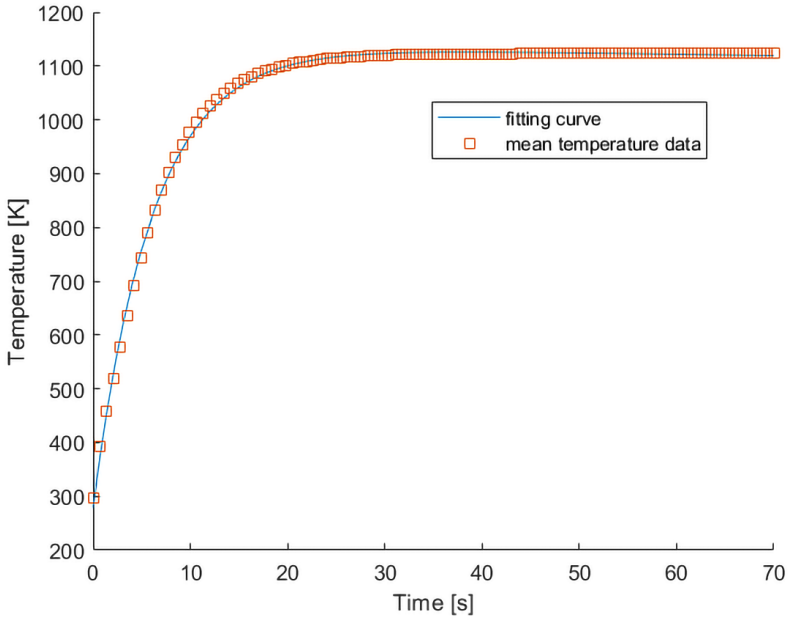

Figure 9. Mean PP particles temperature fitting.

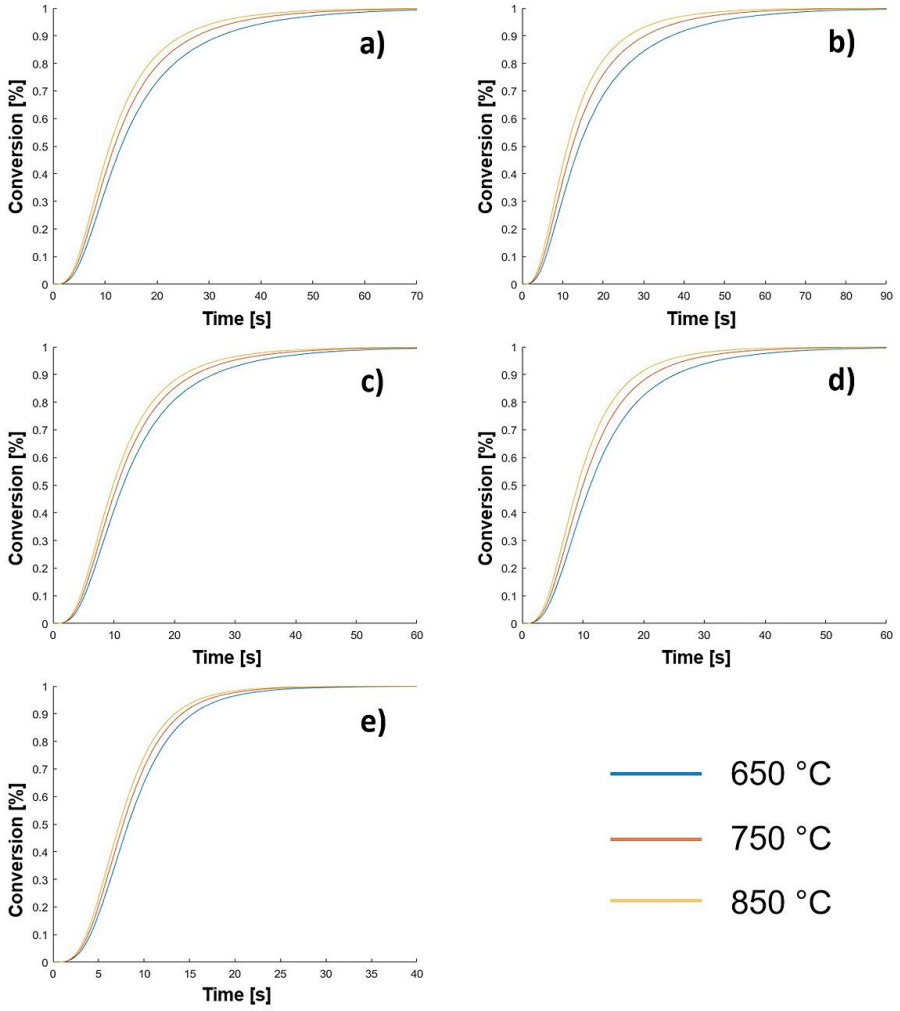

Figure 10. Conversion as predicted by DEV_Model: (**a**) polypropylene; (**b**) poplar; (**c**) wheat straw; (**d**) almond shells; (**e**) OFMSW.

4. Conclusions

The main objective of this work was to analyze and study the devolatilization process, considered as the first step of gasification. The behavior of several solid fuels within a fluidized bed reactor is investigated to develop a model providing important parameters to be implemented in gasification applications.

In particular, the results provide a complete overview of the products of the devolatilization process for various materials and operating temperatures. Moreover, the devolatilization time values were obtained and used to derive the kinetic parameters to describe the devolatilization process and allowed for comparisons of different feed sources on a chemical and kinetic basis.

The development of simplified kinetics permits the description of the overall thermal decomposition process in a fluidized bed, making it simpler to model it in commercial simulation software, even in cases where particles are considered as point-like bodies despite the spherical shape approximation.

By coupling the developed equation related to products' distribution and the DEV_Model, the quantification of the devolatilization process of solid fuels is obtained.

Knowing these data enables their implementation in gasification simulations, although with some limitations. In fact, the model considers only spherical shapes for solid particles, and it does not consider the light hydrocarbons released during devolatilization.

For these reasons, future improvements will be focused on the in-depth analysis of these aspects.

In any case, the developed model and the data presented in this work offer a kind of database representing a starting point for activities oriented to gasification simulation, reactor sizing, and scaling up.

Author Contributions: Conceptualization, A.V. and A.A.P.; methodology, A.V. and A.A.P.; software, A.V.; validation, A.V. and A.A.P.; formal analysis, A.V. and A.A.P.; investigation, A.V. and A.A.P.; resources, A.D.C.; data curation, A.V. and A.A.P.; writing—original draft preparation, A.V. and A.A.P.; writing—review and editing, A.V., A.D.C., P.U.F. and A.A.P.; visualization, A.V., A.D.C., P.U.F. and A.A.P.; supervision, A.D.C. and P.U.F.; project administration, A.D.C.; funding acquisition, A.D.C. All authors have read and agreed to the published version of the manuscript.

Funding: This work was supported by Enereco Spa and PNRR program (DM 352/2022 M4C2) that co-financed a PhD fellowship to the University of L'Aquila (funding number: 91616).

Data Availability Statement: The data presented in this study are available on request from the corresponding author. The data are not publicly available because they are confidential between the company and the authors of this work.

Acknowledgments: The authors kindly acknowledge Nader Jand for his support in the review of the manuscript.

Conflicts of Interest: The authors declare no conflict of interest.

Nomenclature

Property	Symbol	Unit
Apparent activation energy	E_d	J/mol
Bed temperature	T_b	°C
Conversion	χ	-
Devolatilization time	t_d	s
Effective emissivity	ϵ_{eff}	-
Emissivity bed	ϵ_b	-
Gas constant	R	J/mol K
Heat transfer coefficient convection	h	W/(m^2 K)
Initial particles radius	R_p	m
Kinetic "constant"	K_d	s^{-1}
Kinetic parameter for pre-exponential factor fitting	C_1, C_2	-

Parameter for fitting	$a, b, c, d, e, f, g, h, l, m, n, p, q, v$	-
Particle conductivity	k_{eff}	W/(m K)
Particle emissivity	ϵ_p	-
Particle mass	m	g
Particle specific heat	C_p	J/(kg K)
Particles density	r_p	kg/m^3
Pellet volume	V_{Pellet}	m^3
Pre-exponential reference factor	A_d	s^{-1}
Stefan–Boltzman constant	σ	W/(m^2 K^4)

References

1. United Nations. *World Population Prospects 2022, Online Edition*; United Nations: New York, NY, USA, 2022.
2. IEA. *Key World Energy Statistics, IEA, Paris*. 2021. Available online: https://www.iea.org/reports/key-world-energy-statistics-2021 (accessed on 24 September 2023).
3. Lombardi, L.; Carnevale, E.; Corti, A. A review of technologies and performances of thermal treatment systems for energy recovery from waste. *Waste Manag.* **2015**, *37*, 26–44. [CrossRef] [PubMed]
4. Hrbek, J. *Status Report on Thermal Gasification of Biomass and Waste 2021*; IEA Bioenergy: Paris, France, 2022.
5. Papa, A.A.; Taglieri, L.; Gallifuoco, A. Hydrothermal carbonization of waste biomass: An experimental comparison between process layouts. *Waste Manag.* **2020**, *114*, 72–79. [CrossRef]
6. Pandey, B.; Prajapati, Y.K.; Sheth, P.N. Recent progress in thermochemical techniques to produce hydrogen gas from biomass: A state of the art review. *Int. J. Hydrogen Energy* **2019**, *44*, 25384–25415. [CrossRef]
7. Ahmad, A.A.; Zawawi, N.A.; Kasim, F.H.; Inayat, A.; Khasri, A. Assessing the gasification performance of biomass: A review on biomass gasification process conditions, optimization and economic evaluation. *Renew. Sustain. Energy Rev.* **2016**, *53*, 1333–1347. [CrossRef]
8. Burra, K.G.; Gupta, A.K. Synergistic effects in steam gasification of combined biomass and plastic waste mixtures. *Appl. Energy* **2018**, *211*, 230–236. [CrossRef]
9. Di Carlo, A.; Savuto, E.; Foscolo, P.U.; Papa, A.A.; Tacconi, A.; Del Zotto, L.; Aydin, B.; Bocci, E. Preliminary Results of Biomass Gasification Obtained at Pilot Scale with an Innovative 100 kWth Dual Bubbling Fluidized Bed Gasifier. *Energies* **2022**, *15*, 4369. [CrossRef]
10. Molino, A.; Chianese, S.; Musmarra, D. Biomass gasification technology: The state of the art overview. *J. Energy Chem.* **2016**, *25*, 10–25. [CrossRef]
11. Mishra, S.; Upadhyay, R.K. Review on biomass gasification: Gasifiers, gasifying mediums, and operational parameters. *Mater. Sci. Energy Technol.* **2021**, *4*, 329–340. [CrossRef]
12. Papa, A.A.; Savuto, E.; Di Carlo, A.; Tacconi, A.; Rapagnà, S. Synergic Effects of Bed Materials and Catalytic Filter Candle for the Conversion of Tar during Biomass Steam Gasification. *Energies* **2023**, *16*, 595. [CrossRef]
13. Zhang, Z.; Pang, S. Experimental investigation of biomass devolatilization in steam gasification in a dual fluidised bed gasifier. *Fuel* **2017**, *188*, 628–635. [CrossRef]
14. Simone, M.; Biagini, E.; Galletti, C.; Tognotti, L. Evaluation of global biomass devolatilization kinetics in a drop tube reactor with CFD aided experiments. *Fuel* **2009**, *88*, 1818–1827. [CrossRef]
15. Kraft, S.; Kirnbauer, F.; Hofbauer, H. CPFD simulations of an industrial-sized dual fluidized bed steam gasification system of biomass with 8 MW fuel input. *Appl. Energy* **2017**, *190*, 408–420. [CrossRef]
16. Malsegna, B.; Di Giuliano, A.; Gallucci, K. Experimental Study of Absorbent Hygiene Product Devolatilization in a Bubbling Fluidized Bed. *Energies* **2021**, *14*, 2399. [CrossRef]
17. Gomez-Barea, A.; Nilsson, S.; Barrero, F.V.; Campoy, M. Devolatilization of wood and wastes in fluidized bed. *Fuel Process. Technol.* **2010**, *91*, 1624–1633. [CrossRef]
18. Iannello, S.; Foscolo, P.U.; Materazzi, M. Investigation of single particle devolatilization in fluidized bed reactors by X-ray imaging techniques. *Chem. Eng. J.* **2022**, *431*, 133807. [CrossRef]
19. Tokmurzin, D.; Nam, J.Y.; Park, S.J.; Yoon, S.J.; Mun, T.Y.; Yoon, S.M.; Moon, J.H.; Lee, J.G.; Lee, D.H.; Ra, H.W.; et al. Three-Dimensional CFD simulation of waste plastic (SRF) gasification in a bubbling fluidized bed with detailed kinetic chemical model. *Energy Convers. Manag.* **2022**, *267*, 115925. [CrossRef]
20. Xu, J.; Qiao, L. Mathematical Modeling of Coal Gasification Processes in a Well-Stirred Reactor: Effects of Devolatilization and Moisture Content. *Energy Fuels* **2012**, *26*, 5759–5768. [CrossRef]
21. Dymala, T.; Wang, S.; Jarolin, K.; Song, T.; Shen, L.; Dosta, M.; Heinrich, S. MP-PIC Simulation of Biomass Steam Gasification Using Ilmenite as an Oxygen Carrier. *Atmosphere* **2022**, *13*, 1009. [CrossRef]
22. Vitale, A.; Papa, A.A.; Iannello, S.; Ciro, E.; Hatunoglu, A.; Corradetti, V.; Rovelli, N.; Foscolo, P.U.; Carlo, A. Di Devolatilization of Polypropylene Particles in Fluidized Bed. *Energies* **2023**, *16*, 6324. [CrossRef]
23. Kulkarni, M.S.; Dudukovic', M.P. Dynamics of gas phase and solid phase reactions in fixed bed reactors. *Chem. Eng. Sci.* **1996**, *51*, 3083–3088. [CrossRef]

24. Wurzenberger, J.C.; Wallner, S.; Raupenstrauch, H.; Khinast, J.G. Thermal conversion of biomass: Comprehensive reactor and particle modeling. *AIChE J.* **2002**, *48*, 2398–2411. [CrossRef]
25. Byron Bird, R.; Warren, S.E.; Lightfoot, E.N. *Transport Phenomena*, 2nd ed.; John Wiley & Sons Inc.: Hoboken, NJ, USA, 1980.
26. Fogler, H.S. *Elements of Chemical Reaction Engineering*, 6th ed.; Pearson Education International: London, UK, 2020.
27. Pyle, D.L.; Zaror, C.A. Heat transfer and kinetics in the low temperature pyrolysis of solids. *Chem. Eng. Sci.* **1984**, *39*, 147–158. [CrossRef]
28. Rapagnà, S.; di Celso, G.M. Devolatilization of wood particles in a hot fluidized bed: Product yields and conversion rates. *Biomass Bioenergy* **2008**, *32*, 1123–1129. [CrossRef]
29. Yang, H.; Yan, R.; Chen, H.; Lee, D.H.; Zheng, C. Characteristics of hemicellulose, cellulose and lignin pyrolysis. *Fuel* **2007**, *86*, 1781–1788. [CrossRef]
30. Wu, C.; Wang, Z.; Huang, J.; Williams, P.T. Pyrolysis/gasification of cellulose, hemicellulose and lignin for hydrogen production in the presence of various nickel-based catalysts. *Fuel* **2013**, *106*, 697–706. [CrossRef]
31. Cypres, R. Aromatic hydrocarbons formation during coal pyrolysis. *Fuel Process. Technol.* **1987**, *15*, 1–15. [CrossRef]
32. Bockhorn, H.; Hornung, A.; Hornung, U.; Schawaller, D. Kinetic study on the thermal degradation of polypropylene and polyethylene. *J. Anal. Appl. Pyrolysis* **1999**, *48*, 93–109. [CrossRef]